

## Analysis of the thermal instability of laminated composite plates

H. Mataich\*, A. El Amrani<sup>a</sup> and B. El Amrani<sup>b</sup>

*Laboratory of Mathematics, Modeling and Applied Physics, High Normal School,  
Sidi Mohamed Ben Abdellah University, 30040 Fez, Morocco*

*(Received April 24, 2023, Revised December 7, 2023, Accepted December 8, 2023)*

**Abstract.** In this paper, we will analyse the thermo-elastic behavior of the plate element of a structure arranged in a climatically aggressive environment (extreme temperature), we use a refined four-variable thick plate theory to take the shear effect into consideration, the proposed theory less computationally expensive and more accurate so that it incorporates the shear effect into the formulation. The plate is assumed to be simply supported on its four edges, so exact (closed-form) solutions are found according to the Navier expansion, and the governing stability equations and associated boundary conditions of the problem are obtained via the virtual works principle. The plate studied is made of laminated composite materials, so a parametric study is needed to see the effect of different types of parameters and coupling on the critical temperature value causing thermo-elastic instability of the plate and also on the natural frequency of free vibration, as well as for other parameters such as anisotropy, slenderness and aspect ratio of the plate and finally the lamination angle. Numerical results are obtained for specially orthotropic and antisymmetrical plates and are compared with those obtained by other theories in the literature to validate the analysis approach used.

**Keywords:** buckling; composite material; free vibration; instability; laminated plate; Navier series; thermal load

### 1. Introduction

Industrial technological developments, especially in the field of material construction, have been implemented to have new generation materials to overcome limitations in use and meet contemporary challenges in the field of industry, such as space structures for example. For this purpose, composite materials have been introduced for the fabrication of smart laminated composite structures, which are both strong and lightweight as presented by Eswara and Wanhill (2017), Randall and Brian (2012). If these structures are arranged in a climatically aggressive environment (extreme temperature), then, thermal instability is the undesirable phenomenon for these structures, this phenomenon has long been attracting more attention from the researchers Leissa (1987), Majeed and Sadiq (2022).

---

\*Corresponding author, Ph.D., E-mail: hafid.mataich@usmba.ac.ma

<sup>a</sup>Ph.D., E-mail: elamrani.ay@gmail.com

<sup>b</sup>Professor, E-mail: bouchta.elamrani@usmba.ac.ma

### 1.1 Review of the literature

By consulting the literature, the elastic instability or in vibration, is a subject that was treated by researchers in multitudes situations and by the inclusion of different parameters, geometric related to the geometry of the plate or the effect of the distribution of the properties of the materials constituting this plate, where we found studies of the bonds at the boundary of the plate in relation with the instability of the plate. JEYARAJ (2013), Shinde *et al.* (2013), SHINDE *et al.* (2013), Sayyad *et al.* (2014) have dealt with the thermal effect on the dynamic behaviour and elastic instability of isotropic plates, the analysis of the instability of laminated plates made of composite materials in a thermal environment is a subject dealt with by Wen-Chen and Yi-Chen (1989), Also, the stability analysis of a symmetric laminated composite plate has been done by Owhadi and Shariat (2009) and many other researchers have done the same type of work, Ounis *et al.* (2014), Subrata *et al.* (2015), Sayyad *et al.* (2016), Yusuf and Şeref (2018), Madenci *et al.* (2020), Yang *et al.* (2020), Farah *et al.* (2020). Sun (2021) investigated the buckling and vibration performance of a composite laminated plate for elastic connections, Javier Gutiérrez and Chiara (2021) analyse the thermal buckling and mode hopping of metal plates while Rostamijavanani *et al.* (2020) perform thermo-elastic analysis of memory fibre reinforced laminated composite plates and many other studies of similar nature like Bouazza *et al.* (2016), Patro *et al.* (2018), Hammed and Majeed (2019), Farzad *et al.* (2019), Foroutan and Ahmadi (2019). The analysis of thermal instability of functionally graded plates is a topic that was analyzed by Tung (2015), Rasid and Yahaya (2014), Zenkour and Sobhy (2010), Trabelsi *et al.* (2020), Sobhy (2016). Even beams are analysed with the same principles, Zhao *et al.* (2020) presented a thermo-elastic analysis of forced vibrations of a beam, Kobayashi and Sonoda (1991) use a power series expansion method to study the free vibration and buckling of an isotropic plate of conical shape.

## 2. Study problem

In this paper, we will analyse the thermo-elastic behaviour of the plate element of a structure arranged in a climatically aggressive environment (extreme temperature), thus, its free vibration. In this study we use a refined four-variable thick plate theory to take the shear effect into consideration.

### 2.1 Geometric properties of the plate

Let us consider a composite laminated plate of rectangular shape of width  $a$  and length  $b$  with a uniform height  $h$ , this plate consists of  $N_c$  layers, in fact, each layer is the result of reinforcement of a first material (called matrix) by a second one of different properties in the form of fibres, these fibres are arranged, with directions (of angle  $\theta^k$ ), uniformly as it is presented in Fig. 1. The local coordinates of the material  $(x^k, y^k, z^k)$  related to the  $k^{\text{th}}$  layer are oriented at an angle  $\theta^k$  to the axes of the reference frame  $(\hat{x}, \hat{y}, \hat{z})$  The positive ordinate axis  $z$  is fixed downwards such that the ordinates of the two interfaces of the  $k$ -layer are  $z = z_k$  and  $z = z_{k+1}$  as shown in Fig. 2.

### 2.2 Thermal load

The only external load applied on the plate is a thermal load, this load is the resultant of a

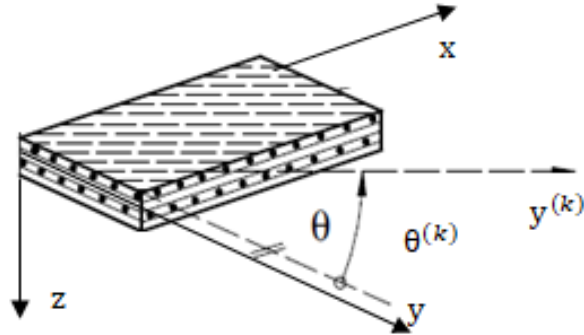


Fig. 1 A laminate with the material and problem coordinate systems

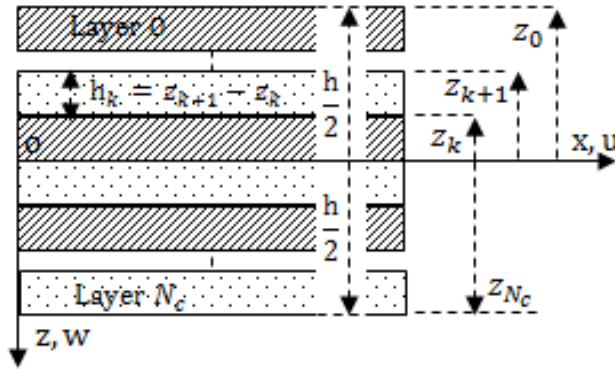


Fig. 2 Coordinate system and layer numbering used for a laminated sheet

temperature field, we assume that its general form according to the Navier development is

$$T(x, y, z) = \sum_{m=1}^{\infty} \sum_{n=1}^{\infty} T(z) \sin(\alpha x) \sin(\beta y) \tag{1}$$

In this study we will consider three cases of distribution of this field through the thickness:

- Steady rise in temperature (UTR):  $T(z) = \Delta T = (T_f - T_i)$
- Linear Temperature Rise (LTR):  $T(z) = T_i + \Delta T(1/2 + z/h)$
- Exponential temperature increase (ETR):  $T(z) = T_i + \Delta T[1 - \cos(\pi/4 + z\pi/h)]$

With, the distribution of the thermal field across the thickness is  $T(z)$ ,  $T_i$  the initial temperature and  $T_f$  the final temperature and  $\Delta T = (T_f - T_i)$  the change in temperature, to simplify the expressions of the equations we put  $\alpha = \frac{m\pi}{a}$  and  $\beta = \frac{n\pi}{b}$ .

### 3. Mathematical formulation of the study problem

#### 3.1 Assumptions

In order to remain in the small deformation range, we consider that the displacements are small in relation to the thickness  $h$ . The displacements in the median plane  $xy$  are  $u_0(x, y) + u^b(x, y) + u^s(x, y)$  in the direction of the  $x$ -axis and  $v_0(x, y) + v^b(x, y) + v^s(x, y)$  in the direction of the  $y$ -

axis are the displacements due to the extension  $u_0(x, y)$ ;  $v_0(x, y)$  bending  $u^b(x, y) = -z w_{0,x}^b$ ;  $v^b(x, y) = -z w_{0,y}^b$  and shear displacements  $u^s(x, y) = -f(z) w_{0,x}^s$ ;  $v^s(x, y) = -f(z) w_{0,y}^s$  transversally the displacement is  $w_0^b(x, y) + w_0^s(x, y)$  is the result of two components, shear  $w_0^s$  and bending  $w_0^b$ . The axial stress along the z-axis,  $\sigma_z$  is very small compared to  $\sigma_x$  and  $\sigma_y$ .

### 3.2 Displacement and deformation fields

We will grant a point  $M(x, y, z)$  of the plate before deformation, after the deformation of the plate, under the temperature field, the point  $M(x, y, z)$  will move according to the following displacement field, according to the study by Alvarez *et al.* (2022)

$$\begin{aligned} u(x, y, z, t) &= u_0(x, y, t) - z w_{0,x}^b(x, y, t) - f(z) w_{0,x}^s(x, y, t) \\ v(x, y, z, t) &= v_0(x, y, t) - z w_{0,y}^b(x, y, t) - f(z) w_{0,y}^s(x, y, t) \\ w(x, y, z, t) &= w_0^b(x, y, t) + w_0^s(x, y, t) \end{aligned} \quad (2)$$

According to the theory used,  $\{u(x, y, z) \quad v(x, y, z) \quad w(x, y, z)\}^T$  is the displacement field in the global reference frame of the laminate  $(\hat{x}, \hat{y}, \hat{z})$ . The function  $f(z)$  is the model for the development of the shear effect through the thickness, we will base on our proposed model and to validate we use a first model of third order shear deformations of Reddy (HPT), Belkacem *et al.* (2016), the second model is that of sinusoidal deformations of Touratier (SPT), Yang *et al.* (2020)

$$\begin{aligned} (\text{Present}): \quad f(z) &= h \sin(\sin(\pi z/h))/\pi \\ (\text{HPT}) \quad &: f(z) = -(4z^3/3h^2) - z \\ (\text{SPT}) \quad &: f(z) = (h/\pi)\sin(\pi z/h) \end{aligned} \quad (3)$$

Without taking into account the second-order (Von Karman) or higher deformation terms, then the linear deformation field takes the following form for the  $k^{\text{th}}$  layer

$$\begin{aligned} \varepsilon_x^{(k)} &= u_{0,x} - z w_{0,xx}^b - f(z) w_{0,xx}^s &= \varepsilon_x^0 + z k_x^b + f(z) k_x^s \\ \varepsilon_y^{(k)} &= v_{0,y} - z w_{0,yy}^b - f(z) w_{0,yy}^s &= \varepsilon_y^0 + z k_y^b + f(z) k_y^s \\ \gamma_{xy}^{(k)} &= u_{0,y} + v_{0,x} - 2z w_{0,xy}^b - 2f(z) w_{0,xy}^s &= \gamma_{xy}^0 + z k_{xy}^b + f(z) k_{xy}^s \\ \gamma_{yz}^{(k)} &= (1 - f(z),_z) w_{0,y}^s &= (1 - f(z),_z) \gamma_{yz}^s \\ \gamma_{xz}^{(k)} &= (1 - f(z),_z) w_{0,x}^s &= (1 - f(z),_z) \gamma_{xz}^s \end{aligned} \quad (4)$$

Under the above assumptions in this methodology  $\{\varepsilon_x, \varepsilon_y, \gamma_{xy}, \gamma_{yz}, \gamma_{xz}\}^{(k)T}$  is the deformation field related to the point  $M(x, y, z)$  of the  $k^{\text{th}}$  layer.

### 3.3 Constitutive equations, stress-strain

We apply Hooke's law to the case of a linear and orthotropic elastic material. In the presence of a thermal load and for each layer, the stress field takes the following form

$$\begin{Bmatrix} \sigma_x \\ \sigma_y \\ \tau_{xy} \end{Bmatrix}^{(k)} = \begin{bmatrix} \bar{Q}_{11} & \bar{Q}_{12} & \bar{Q}_{16} \\ \bar{Q}_{12} & \bar{Q}_{22} & \bar{Q}_{26} \\ \bar{Q}_{16} & \bar{Q}_{26} & \bar{Q}_{66} \end{bmatrix}^{(k)} \begin{Bmatrix} \varepsilon_x \\ \varepsilon_y \\ \gamma_{xy} \end{Bmatrix}^{(k)} - \begin{Bmatrix} \alpha_x T(z) \\ \alpha_y T(z) \\ 2\alpha_{xy} T(z) \end{Bmatrix}^{(k)}$$

Table 1 Values of the undesigned engineering constants of the materials used

Material Properties	$E_1$ (GPa)	$E_2$ (GPa)	$G_{12}$ (GPa)	$G_{13}$ (GPa)	$G_{23}$ (GPa)	$\nu_{12}$	$\alpha_1(1/^\circ C)$	$\alpha_2(1/^\circ C)$
Graphite-Epoxy	$40.E_2$	6.92	$0.6.E_2$	$0.6.E_2$	$0.5.E_2$	0.25	$1,14.10^{-6}$	$1,14.10^{-6}$

$$\text{and } \begin{Bmatrix} \tau_{yz} \\ \tau_{xz} \end{Bmatrix}^{(k)} = \begin{bmatrix} \bar{Q}_{44} & \bar{Q}_{45} \\ \bar{Q}_{45} & \bar{Q}_{55} \end{bmatrix}^{(k)} \begin{Bmatrix} \gamma_{yz} \\ \gamma_{xz} \end{Bmatrix}^{(k)} \quad (5)$$

The stress field  $\{\sigma_x, \sigma_y, \tau_{xy}, \tau_{yz}, \tau_{xz}\}^T$  in the  $k^{\text{th}}$  layer will be determined using the transformed stiffnesses Eq. (8) of the material

$$\begin{aligned} \bar{Q}_{11}^{(k)} &= Q_{11} \cos^4 \theta^{(k)} + 2(Q_{12} + 2Q_{66}) \cos^2 \theta^{(k)} \sin^2 \theta^{(k)} + Q_{22} \sin^4 \theta^{(k)} \\ \bar{Q}_{12}^{(k)} &= Q_{12} \cos^4 \theta^{(k)} + (Q_{11} + Q_{22} - 4Q_{66}) \cos^2 \theta^{(k)} \sin^2 \theta^{(k)} + Q_{12} \sin^4 \theta^{(k)} \\ \bar{Q}_{22}^{(k)} &= Q_{22} \cos^4 \theta^{(k)} + 2(Q_{12} + 2Q_{66}) \cos^2 \theta^{(k)} \sin^2 \theta^{(k)} + Q_{11} \sin^4 \theta^{(k)} \\ \bar{Q}_{16}^{(k)} &= (Q_{11} - Q_{12} - 2Q_{66}) \cos^3 \theta^{(k)} \sin \theta^{(k)} + (2Q_{66}^{(k)} + Q_{12} - Q_{22}) \cos \theta^{(k)} \sin^3 \theta^{(k)} \\ \bar{Q}_{26}^{(k)} &= (Q_{11} - Q_{12} - 2Q_{66}) \cos \theta^{(k)} \sin^3 \theta^{(k)} + (2Q_{66} + Q_{12} - Q_{22}) \cos^3 \theta^{(k)} \sin \theta^{(k)} \\ \bar{Q}_{66}^{(k)} &= (Q_{11} + Q_{22} - 2Q_{12} - 2Q_{66}) \cos^2 \theta^{(k)} \sin^2 \theta^{(k)} + Q_{66} (\cos^4 \theta^{(k)} + \sin^4 \theta^{(k)}) \\ \bar{Q}_{44}^{(k)} &= Q_{44} \cos^2 \theta^{(k)} + Q_{55} \sin^2 \theta^{(k)} \\ \bar{Q}_{45}^{(k)} &= (Q_{55} - Q_{44}) \cos \theta^{(k)} \sin \theta^{(k)} \quad \bar{Q}_{55}^{(k)} = Q_{55} \cos^2 \theta^{(k)} + Q_{44} \sin^2 \theta^{(k)} \end{aligned} \quad (6)$$

The coefficient of thermal expansion  $\alpha_x, \alpha_y$  and  $\alpha_{xy}$  transformed into the global axis system, with

$$\begin{aligned} \alpha_x^{(k)} &= \alpha_1 \cos^2 \theta^{(k)} + \alpha_2 \sin^2 \theta^{(k)} & \alpha_y^{(k)} &= \alpha_1 \sin^2 \theta^{(k)} + \alpha_2 \cos^2 \theta^{(k)} \\ \alpha_{xy}^{(k)} &= (\alpha_1 - \alpha_2) \sin \theta^{(k)} \cos \theta^{(k)} \end{aligned} \quad (7)$$

The laws of elasticity allow the material stiffnesses to be related to  $Q_{ij}^{(k)}$ ;  $i, j = 1, 2, 4, 5, 6$  to the engineering constants as presented in the following formulas

$$Q_{11} = \frac{E_1}{1 - \nu_{12}\nu_{21}}; \quad Q_{12} = \frac{\nu_{12}E_2}{1 - \nu_{12}\nu_{21}}; \quad Q_{22} = \frac{E_2}{1 - \nu_{12}\nu_{21}}; \quad Q_{66} = G_{12}; \quad Q_{44} = G_{23}; \quad Q_{55} = G_{13} \quad (8)$$

In the case of plane stress, the reduced stiffnesses require the following independent engineering constants:

The resultant forces and moments are found by integrating, through the thickness of the plate, the stresses taking into account the adopted theory, as follows

$$\begin{aligned} \begin{bmatrix} N_x & N_y & N_{xy} \\ M_x^b & M_y^b & M_{xy}^b \\ M_x^s & M_y^s & M_{xy}^s \end{bmatrix} &= \sum_{k=1}^{N_c} \left( \int_{z_k}^{z_{k+1}} \begin{Bmatrix} 1 \\ z \\ f(z) \end{Bmatrix} (\sigma_x, \sigma_y, \tau_{xy})^{(k)} dz \right) \\ \text{and } \begin{Bmatrix} S_{yz}^s \\ S_{xy}^s \end{Bmatrix} &= \sum_{k=1}^{N_c} \left( \int_{z_k}^{z_{k+1}} \left( 1 - \frac{df(z)}{dz} \right) \begin{Bmatrix} \tau_{yz} \\ \tau_{xz} \end{Bmatrix}^{(k)} dz \right) \end{aligned} \quad (9)$$

Similarly, to find the field of thermal forces and moments, but in this case using the thermal properties of the plate and the expression for the temperature distribution

$$\begin{bmatrix} N_x^T = N_0^T & N_y^T = N_0^T & N_{xy}^T = 0 \\ M_x^{bT} = M_0^{bT} & M_y^{bT} = M_0^{bT} & M_{xy}^{bT} = 0 \\ M_x^{sT} = M_0^{sT} & M_y^{sT} = M_0^{sT} & M_{xy}^{sT} = 0 \end{bmatrix} = \sum_{k=1}^{N_c} \int_{z_k}^{z_{k+1}} \frac{E^{(k)}}{1-\nu^{(k)}} T(x, y, z) \begin{Bmatrix} 1 \\ z \\ f(z) \end{Bmatrix} \{\alpha_0, \alpha_0, 0\}^{(k)} dz \quad (10)$$

**N.B.:** From the data in Table 1, we have  $\alpha_1 = \alpha_2$  and from the transformations in Eq. (5) the transformed thermal expansion coefficients are:  $\alpha_x = \alpha_y = \alpha_0$  and  $\alpha_{yx} = 0$

After doing the integrations Eq. (9) and Eq. (10) we get eleven resultant forces and moments, as a function of eleven membrane deformations and curvatures, these results are organized in the following matrices Eq. (11) and Eq.

$$\begin{pmatrix} N_x \\ N_y \\ N_{xy} \\ M_x^b \\ M_y^b \\ M_{xy}^b \\ M_x^s \\ M_y^s \\ M_{xy}^s \end{pmatrix} = \begin{bmatrix} A_{11} & A_{12} & A_{16} \\ A_{12} & A_{22} & A_{26} \\ A_{16} & A_{26} & A_{66} \\ B_{11} & B_{12} & B_{16} \\ B_{12} & B_{22} & B_{26} \\ B_{16} & B_{26} & B_{66} \\ D_{11} & D_{12} & D_{16} \\ D_{12} & D_{22} & D_{26} \\ D_{16} & D_{26} & D_{66} \\ B_{11}^s & B_{12}^s & B_{16}^s \\ B_{12}^s & B_{22}^s & B_{26}^s \\ B_{16}^s & B_{26}^s & B_{66}^s \\ D_{11}^s & D_{12}^s & D_{16}^s \\ D_{12}^s & D_{22}^s & D_{26}^s \\ D_{16}^s & D_{26}^s & D_{66}^s \\ H_{11}^s & H_{12}^s & H_{16}^s \\ H_{12}^s & H_{22}^s & H_{26}^s \\ H_{16}^s & H_{26}^s & H_{66}^s \end{bmatrix} \begin{pmatrix} \varepsilon_x^0 \\ \varepsilon_y^0 \\ \gamma_{xy}^0 \\ \kappa_x^b \\ \kappa_y^b \\ \kappa_{xy}^b \\ \kappa_x^s \\ \kappa_y^s \\ \kappa_{xy}^s \end{pmatrix} - \begin{pmatrix} N_0^T \\ N_0^T \\ 0 \\ M_0^{bT} \\ M_0^{bT} \\ 0 \\ M_0^{sT} \\ M_0^{sT} \\ 0 \end{pmatrix} \quad (11)$$

$$\begin{pmatrix} S_{yz}^s \\ S_{xz}^s \end{pmatrix} = \begin{bmatrix} A_{44}^s & A_{45}^s \\ A_{45}^s & A_{55}^s \end{bmatrix} \begin{pmatrix} \gamma_{yz}^s \\ \gamma_{xz}^s \end{pmatrix} \quad (12)$$

The normal and coupling stiffnesses  $\{A_{ij}, B_{ij}, D_{ij}, B_{ij}^s, D_{ij}^s, H_{ij}^s, A_{ij}^s\}$  and coupling stiffnesses are calculated taking into account the layering of each layer and the properties of the materials used, as follows

$$\{A_{ij}, B_{ij}, D_{ij}, B_{ij}^s, D_{ij}^s, H_{ij}^s\} = \sum_{k=1}^{N_c} \int_{z_k}^{z_{k+1}} Q_{ij}^{(k)} \{1, z, z^2, f(z), zf(z), f^2(z)\} dz; \quad i, j = 1, 2, 6 \quad (13)$$

$$A_{ij}^s = \sum_{k=1}^{N_c} \int_{z_k}^{z_{k+1}} Q_{ij}^{(k)} \left(1 - \frac{df(z)}{dz}\right)^2 dz; \quad i, j = 4, 5 \quad (14)$$

### 3.4 Stability governing equations

To find the equilibrium equations of the plate we can express them using the principle of virtual works in its dynamic version, as, Yang *et al.* (2020)

$$\int \delta(U + V - E) dt = 0 \quad (15)$$

Where, the internal strain energy  $\delta U$  the virtual work  $\delta V$  done by the thermal forces caused by the thermal stresses applied in the plane and  $\delta E$  is the kinetic energy, these quantities are integrated as follows:

- The deformation energy

$$U = \iint \left[ \int_{-h/2}^{+h/2} [N_x \varepsilon_x^0 + N_y \varepsilon_y^0 + N_{xy} \gamma_{xy}^0 + M_x^b \kappa_x^b + M_y^b \kappa_y^b + M_{xy}^b \kappa_{xy}^b + M_x^s \kappa_x^s + M_y^s \kappa_y^s + M_{xy}^s \kappa_{xy}^s + S_{yz}^s \gamma_{yz}^s + S_{xz}^s \gamma_{xz}^s] dz \right] dx dy \quad (16)$$

- The work of the forces caused by the thermal field in the

$$V = - \iint [F_x(w_{0,xx}^b + w_{0,xx}^s) + 2F_{xy}(w_{0,xy}^b + w_{0,xy}^s) + F_y(w_{0,yy}^b + w_{0,yy}^s)] dx dy \quad (17)$$

- The kinetic energy of the plate

$$E = \frac{1}{2} \iint \{ \delta u (I_1 \ddot{u} - I_2 \ddot{w}_{0,x}^b - I_4 \ddot{w}_{0,x}^s) + \delta v (I_1 \ddot{v} - I_2 \ddot{w}_{0,y}^b - I_4 \ddot{w}_{0,y}^s) + \delta w_0^b [I_1 (\ddot{w}_0^b + \ddot{w}_0^s) + I_2 (\ddot{u}_{,x} + \ddot{v}_{,y}) - I_3 (\ddot{w}_{0,xx}^b + \ddot{w}_{0,yy}^b) - I_5 (\ddot{w}_{0,xx}^s + \ddot{w}_{0,yy}^s)] + \delta w_0^s [I_1 (\ddot{w}_0^b + \ddot{w}_0^s) + I_4 (\ddot{u}_{,x} + \ddot{v}_{,y}) - I_5 (\ddot{w}_{0,xx}^b + \ddot{w}_{0,yy}^b) - I_6 (\ddot{w}_{0,xx}^s + \ddot{w}_{0,yy}^s)] \} dx dy \quad (18)$$

We substitute equations Eq. (16), Eq. (17) and Eq. (18) into equation (15) and integrate through the thickness, the latter equation Eq. (15) can be rewritten as

$$\iint \{ [N_x \delta \varepsilon_x^0 + N_y \delta \varepsilon_y^0 + N_{xy} \delta \varepsilon_{xy}^0 + M_x^b \delta k_x^b + M_y^b \delta k_y^b + M_{xy}^b \delta k_{xy}^b + M_x^s \delta k_x^s + M_y^s \delta k_y^s + M_{xy}^s \delta k_{yz}^s + S_{yz}^s \delta \gamma_{yz}^s + S_{xz}^s \delta \gamma_{xz}^s] - \{ F_x (w_{0,xx}^b + w_{0,xx}^s) + 2F_{xy} (w_{0,xy}^b + w_{0,xy}^s) + F_y (w_{0,yy}^b + w_{0,yy}^s) \} + \{ \delta u I_1 \ddot{u} + \delta v I_1 \ddot{v} + \delta w_0^b [I_1 (\ddot{w}_0^b + \ddot{w}_0^s) - I_2 (\ddot{w}_{0,xx}^b + \ddot{w}_{0,yy}^b) - I_3 (\ddot{w}_{0,xx}^s + \ddot{w}_{0,yy}^s)] + \delta w_0^s [I_1 (\ddot{w}_0^b + \ddot{w}_0^s) - I_3 (\ddot{w}_{0,xx}^b + \ddot{w}_{0,yy}^b) - I_4 (\ddot{w}_{0,xx}^s + \ddot{w}_{0,yy}^s)] \} \} dx dx = 0 \quad (19)$$

The thermal compression forces in the plane  $F_x$  and  $F_y$  plane now represent loads instead of reaction forces

$$\{F_x, F_y, F_{xy}\} = \sum_{k=1}^{N_c} \frac{E^{(k)}}{1-\nu^{(k)}} \int_{z_k}^{z_{k+1}} T(z) dz \{ \alpha_0, \alpha_0, 0 \}^{(k)} \quad (20)$$

The inertias of the plate are defined as (21), where  $\rho^{(k)}$  is the mass per unit volume for the  $k^{\text{th}}$  layer.

$$\{I_1, I_2, I_3, I_4, I_5, I_6\} = \sum_{k=1}^{N_c} \int_{z=z_k}^{z_{k+1}} \rho^{(k)} (1, z, z^2, f(z), zf(z), f(z)^2) dz \quad (21)$$

The governing equilibrium equations can be determined from Eq. (19) by integration by parts, so

$$\begin{aligned} \delta u \neq 0: & \quad N_{x,x} + N_{xy,y} = I_1 \ddot{u} - I_2 \ddot{w}_{0,x}^b - I_4 \ddot{w}_{0,x}^s \\ \delta v \neq 0: & \quad N_{xy,x} + N_{y,y} = I_1 \ddot{v} - I_2 \ddot{w}_{0,y}^b - I_4 \ddot{w}_{0,y}^s \\ \delta w_b \neq 0: & \quad M_{x,xx}^b + 2M_{xy,xy}^b + M_{y,yy}^b + F_x w_{0,xx}^b + F_y w_{0,yy}^b = I_2 (\ddot{u}_{,x} + \ddot{v}_{,y}) + I_1 (\ddot{w}_0^b + \ddot{w}_0^s) - I_3 (\ddot{w}_{0,xx}^b + \ddot{w}_{0,yy}^b) - I_5 (\ddot{w}_{0,xx}^s + \ddot{w}_{0,yy}^s) \\ \delta w_s \neq 0: & \quad M_{x,xx}^s + 2M_{xy,xy}^s + M_{y,yy}^s + F_x w_{0,xx}^s + 2F_{xy} w_{0,xy}^s + F_y w_{0,yy}^s + S_{xz,x}^s + S_{yz,y}^s = I_4 (\ddot{u}_{,x} + \ddot{v}_{,y}) + I_1 (\ddot{w}_0^b + \ddot{w}_0^s) - I_5 (\ddot{w}_{0,xx}^b + \ddot{w}_{0,yy}^b) - I_6 (\ddot{w}_{0,xx}^s + \ddot{w}_{0,yy}^s) \end{aligned} \quad (22)$$

### 3.5 Stability governing equations in terms of displacement

Based on the stability equations Eq. (22) found in the previous section, we substitute the resultant forces and resultant moments from the expressions in Eq. (11), and then exploit the expressions for deformations found in Eq. (4), we finally arrive at four stability equations in terms of displacements, as follows

$$\begin{aligned}
& A_{11}u_{0,xx} + 2A_{16}u_{0,xy} + A_{66}u_{0,yy} + A_{16}v_{0,xx} + (A_{12} + A_{66})v_{0,xy} + A_{26}v_{0,yy} - \\
& B_{11}w_{0,xxx}^b - (B_{12} + 2B_{66})w_{0,xyy}^b - 3B_{16}w_{0,xxxy}^b - B_{26}w_{0,yyy}^b - B_{11}^s w_{0,xxx}^s - (B_{12}^s + \\
& 2B_{66}^s)w_{0,xyy}^s - 3B_{16}^s w_{0,xxxy}^s - B_{26}^s w_{0,yyy}^s - I_1 \ddot{u} + I_2 \ddot{w}_{0,x}^b + I_4 \ddot{w}_{0,x}^s = N_{0,x}^T
\end{aligned} \quad (23)$$

$$\begin{aligned}
& A_{16}u_{0,xx} + (A_{12} + A_{66})u_{0,xy} + A_{26}u_{0,yy} + A_{22}v_{0,yy} + 2A_{26}v_{0,xy} + A_{66}v_{0,xx} - \\
& B_{22}w_{0,yyy}^b - (B_{12} + 2B_{66})w_{0,xxxy}^b - 3B_{26}w_{0,xyy}^b - B_{16}w_{0,xxx}^b - B_{22}^s w_{0,yyy}^s - (B_{12}^s + \\
& 2B_{66}^s)w_{0,xxxy}^s - 3B_{26}^s w_{0,xyy}^s - B_{16}^s w_{0,xxx}^s - I_1 \ddot{v} + I_2 \ddot{w}_{0,y}^b + I_4 \ddot{w}_{0,y}^s = N_{0,y}^T
\end{aligned} \quad (24)$$

$$\begin{aligned}
& -B_{11}u_{0,xxx} - (B_{12} + 2B_{66})u_{0,xyy} - 3B_{16}u_{0,xxxy} - B_{26}u_{0,yyy} - B_{22}v_{0,yyy} - (B_{12} + \\
& 2B_{66})v_{0,xxxy} - 3B_{26}v_{0,xyy} - B_{16}v_{0,xxx} + D_{11}w_{0,xxxx}^b + 2(D_{12} + 2D_{66})w_{0,xxxy}^b + \\
& 4D_{16}w_{0,xxxxy}^b + 4D_{26}w_{0,xyyy}^b + D_{22}w_{0,yyy}^b + F_x w_{0,xx}^b + F_y w_{0,yy}^b + D_{11}^s w_{0,xxxx}^s + \\
& 2(D_{12}^s + 2D_{66}^s)w_{0,xxxy}^s + 4D_{16}^s w_{0,xxxxy}^s + 4D_{26}^s w_{0,xyyy}^s + D_{22}^s w_{0,yyy}^s + F_x w_{0,xx}^s + F_y w_{0,yy}^s + \\
& I_2(\ddot{u}_x + \ddot{v}_y) + I_1(\ddot{w}_0^b + \ddot{w}_0^s) - I_3(\ddot{w}_{0,xx}^b + \ddot{w}_{0,yy}^b) - I_5(\ddot{w}_{0,xx}^s + \ddot{w}_{0,yy}^s) = -M_{0,xx}^{bT} - M_{0,yy}^{bT}
\end{aligned} \quad (25)$$

$$\begin{aligned}
& -B_{11}^s u_{0,xxx} - (B_{12}^s + 2B_{66}^s)u_{0,xyy} - 3B_{16}^s u_{0,xxxy} - B_{26}^s u_{0,yyy} - B_{22}^s v_{0,yyy} - (B_{12}^s + \\
& 2B_{66}^s)v_{0,xxxy} - 3B_{26}^s v_{0,xyy} - B_{16}^s v_{0,xxx} + D_{11}^s w_{0,xxxx}^b + 2(D_{12}^s + 2D_{66}^s)w_{0,xxxy}^b + \\
& 4D_{16}^s w_{0,xxxxy}^b + 4D_{26}^s w_{0,xyyy}^b + D_{22}^s w_{0,yyy}^b + F_x w_{0,xx}^b + F_y w_{0,yy}^b + H_{11}^s w_{0,xxxx}^s + \\
& 2(H_{12}^s + 2H_{66}^s)w_{0,xxxy}^s + 4H_{16}^s w_{0,xxxxy}^s + 4H_{26}^s w_{0,xyyy}^s + H_{22}^s w_{0,yyy}^s + A_{55}^s w_{0,xx}^s + \\
& 2A_{45}^s w_{0,xy}^s + A_{44}^s w_{0,yy}^s + F_x w_{0,xx}^s + F_y w_{0,yy}^s + I_4(\ddot{u}_x + \ddot{v}_y) + I_1(\ddot{w}_0^b + \ddot{w}_0^s) - \\
& I_5(\ddot{w}_{0,xx}^b + \ddot{w}_{0,yy}^b) - I_6(\ddot{w}_{0,xx}^s + \ddot{w}_{0,yy}^s) = -M_{0,xx}^{sT} - M_{0,yy}^{sT}
\end{aligned} \quad (26)$$

## 4. Analytical solutions to the problem

### 4.1 Matrix writing of the problem

In the case of specially orthotropic or antisymmetric layering, we use the Navier approximations given in Eq. (27) for the displacement field, for further details and clarification of the boundary conditions please see reference Shiau and Wu (1997).

Antisymmetrical cross-pleated

$$\begin{aligned}
u_0(x, y) &= \sum_{m=1}^{\infty} \sum_{n=1}^{\infty} e^{j\omega t} U_{mn} \cdot \cos(\alpha x) \sin(\beta y). \\
v_0(x, y) &= \sum_{m=1}^{\infty} \sum_{n=1}^{\infty} e^{j\omega t} V_{mn} \cdot \sin(\alpha x) \cos(\beta y).
\end{aligned}$$

And for all stratifications

$$\begin{aligned}
w_0^b(x, y) &= \sum_{m=1}^{\infty} \sum_{n=1}^{\infty} e^{j\omega t} W_{mn}^b \cdot \sin(\alpha x) \sin(\beta y) \\
w_0^s(x, y) &= \sum_{m=1}^{\infty} \sum_{n=1}^{\infty} e^{j\omega t} W_{mn}^s \cdot \sin(\alpha x) \sin(\beta y)
\end{aligned} \quad \text{for } \alpha = \frac{m\pi}{a} \text{ and } \beta = \frac{n\pi}{b} \quad (27)$$

We substitute the field (27) in the stability equations Eq. (23)-Eq. (26), the resulting expressions are organized in a matrix writing in the form

$$[R]\{d_{mn}\} - \omega^2[M]\{d_{mn}\} = \{F_{mn}\} \quad (28)$$

In this writing,  $[R]$  is the symmetric matrix of modified rigidities,  $[M]$  is the symmetric mass matrix,  $\{d_{mn}\}$  the vector of unknown displacements and the vector of thermal forces acting on the plate is  $\{F_{mn}\}$  with

$$[R] = \begin{bmatrix} R_{11} & R_{12} & R_{13} & R_{14} \\ R_{12} & R_{22} & R_{23} & R_{24} \\ R_{13} & R_{23} & R_{33} - F & R_{34} - F \\ R_{14} & R_{24} & R_{34} - F & R_{44} - F \end{bmatrix}, [M] = \begin{bmatrix} M_{11} & M_{12} & M_{13} & M_{14} \\ M_{12} & M_{22} & M_{23} & M_{24} \\ M_{13} & M_{23} & M_{33} & M_{34} \\ M_{14} & M_{24} & M_{34} & M_{44} \end{bmatrix}$$

$$\text{and } \{d_{mn}\} = \{U_{mn}, V_{mn}, W_{mn}^b, W_{mn}^s\}^T \quad \{F_{mn}\} = \{F_{mn}^1, F_{mn}^2, F_{mn}^3, F_{mn}^4\}^T$$

The rigidities ( $R_{ij}$ ) are determined after substituting the field Eq. (27) into Eq. (23) to Eq. (26), then

$$\begin{aligned} R_{11} &= A_{11}\alpha^2 + 2A_{16}\alpha\beta + A_{66}\beta^2 \\ R_{12} &= A_{16}\alpha^2 + (A_{12} + A_{66})\alpha\beta + A_{26}\beta^2 \\ R_{13} &= -B_{11}\alpha^3 - (B_{12} + 2B_{66})\alpha\beta^2 - 3B_{16}\alpha^2\beta - B_{26}\beta^3 \\ R_{14} &= -B_{11}^s\alpha^3 - (B_{12}^s + 2B_{66}^s)\alpha\beta^2 - 3B_{16}^s\alpha^2\beta - B_{26}^s\beta^3 \\ R_{22} &= A_{22}\beta^2 + 2A_{26}\alpha\beta + A_{66}\alpha^2 \\ R_{23} &= -B_{22}\beta^3 - (B_{12} + 2B_{66})\alpha^2\beta - 3B_{26}\alpha\beta^2 - B_{16}\alpha^3 \\ R_{24} &= -B_{22}^s\beta^3 - (B_{12}^s + 2B_{66}^s)\alpha^2\beta - 3B_{26}^s\alpha\beta^2 - B_{16}^s\alpha^3 \\ R_{33} &= D_{11}\alpha^4 + 2(D_{12} + 2D_{66})\alpha^2\beta^2 + 4D_{16}\alpha^3\beta + 4D_{26}\alpha\beta^3 + D_{22}\beta^4 \\ R_{34} &= D_{11}^s\alpha^4 + 2(D_{12}^s + 2D_{66}^s)\alpha^2\beta^2 + 4D_{16}^s\alpha^3\beta + 4D_{26}^s\alpha\beta^3 + D_{22}^s\beta^4 \\ R_{44} &= H_{11}^s\alpha^4 + 2(H_{12}^s + 2H_{66}^s)\alpha^2\beta^2 + 4H_{16}^s\alpha^3\beta + 4H_{26}^s\alpha\beta^3 + H_{22}^s\beta^4 + A_{55}^s\alpha^2 \\ &\quad + 2A_{45}^s\alpha\beta + A_{44}^s\beta^2 \end{aligned} \quad (29)$$

In order for us to develop closed form Navier solutions, we need to have a zero thermal shear residual stress  $F_{xy} = 0$  (this condition is verified by the numerical values in Table 1). Due to simplification of the parametric study, we set  $F_x = \xi F_y$ . In order to have a uni-axial thermal effect, we will take  $\xi = 0$  and  $\xi = 1$  for a bi-axial effect, then

$$F = F_x\alpha^2 + F_y\beta^2 = F_x(\alpha^2 + \xi\beta^2) \quad (30)$$

The coefficients ( $M_{ij}$ ) are determined after applying the field Eq. (27) in Eq. (23) to Eq. (26), then

$$\begin{aligned} M_{11} &= -I_1 & M_{12} &= 0 & M_{13} &= \alpha I_2 & M_{14} &= \alpha I_4 & M_{22} &= -I_1 \\ M_{23} &= \beta I_2 & M_{24} &= \beta I_4 & M_{33} &= I_1 - I_3(\alpha^2 + \beta^2) & M_{34} &= I_1 - I_5(\alpha^2 + \beta^2) \\ & & M_{34} &= I_1 - I_5(\alpha^2 + \beta^2) & M_{44} &= I_1 - I_6(\alpha^2 + \beta^2) \end{aligned} \quad (31)$$

The terms of the thermal force vector are determined as follows

Table 2 Expression of the thermal load according to the temperature distribution through the thickness

Temperature distribution	Thermal load
Regular increase (UTR)	$F_x = \Delta T \frac{E_2\alpha_0}{1-\nu_{12}} \int_{-h/2}^{h/2} dz.$
Linear increase (LTR)	$F_x = \frac{E_2\alpha_0}{1-\nu_{12}} T_i \int_{-h/2}^{h/2} dz + \Delta T \frac{E_2\alpha_0}{1-\nu_{12}} \int_{-h/2}^{h/2} \left(\frac{1}{2} + \frac{z}{h}\right) dz.$
Exponential increase (ETR)	$F_x = \frac{E_2\alpha_0}{1-\nu_{12}} T_i \int_{-h/2}^{h/2} dz + \Delta T \frac{E_2\alpha_0}{1-\nu_{12}} \int_{-h/2}^{h/2} \left[1 - \cos\left(\frac{\pi}{4} + \frac{z\pi}{h}\right)\right] dz.$

Table 3 Expression of critical thermal change according to temperature distribution across the thickness

Temperature distribution	Thermal load
Regular increase (UTR)	$\Delta T_{cr} = \frac{1}{(\alpha^2 + \xi \beta^2) \kappa_{utr}} \frac{R_{34}R_{43} - R_{33}R_{44}}{(R_{34} + R_{43} - R_{33} - R_{44})}$
Linear increase (LTR)	$\Delta T_{cr} = \frac{1}{(\alpha^2 + \xi \beta^2) \kappa_{ltr}} \frac{R_{34}R_{43} - R_{33}R_{44}}{(R_{34} + R_{43} - R_{33} - R_{44})} - \frac{\kappa_{utr}}{\kappa_{ltr}} T_i$
Exponential increase (STR)	$\Delta T_{cr} = \frac{1}{(\alpha^2 + \xi \beta^2) \kappa_{str}} \frac{R_{34}R_{43} - R_{33}R_{44}}{(R_{34} + R_{43} - R_{33} - R_{44})} - \frac{\kappa_{utr}}{\kappa_{str}} T_i$

$$\begin{aligned}
F_{mn}^1 &= \alpha \sum_{k=1}^{N_c} \int_{z_k}^{z_{k+1}} \frac{E^{(k)}}{1-\nu^{(k)}} T(z) dz & F_{mn}^2 &= \beta \sum_{k=1}^{N_c} \int_{z_k}^{z_{k+1}} \frac{E^{(k)}}{1-\nu^{(k)}} T(z) dz \\
F_{mn}^3 &= -(\alpha^2 + \beta^2) \sum_{k=1}^{N_c} \int_{z_k}^{z_{k+1}} \frac{E^{(k)}}{1-\nu^{(k)}} z T(z) dz & F_{mn}^4 &= -(\alpha^2 + \beta^2) \sum_{k=1}^{N_c} \int_{z_k}^{z_{k+1}} \frac{E^{(k)}}{1-\nu^{(k)}} f(z) T(z) dz
\end{aligned} \quad (32)$$

But we do not need these terms since we are looking for critical values for the elastic stability and natural frequency in the case of free plate vibrations.

#### 4.2 Critical buckling temperature of laminated composite plates

The solution of the buckling problem requires a time fixation, i.e., the time must be constant, furthermore, the governing equations of the plate under static buckling are obtained by eliminating the thermal loads Eq. (10) and the inertia terms ( $I_1, I_2, I_3, I_4$ ) in Eq. (23) to Eq. (26), then the system Eq. (28) simplifies to

$$[R]\{d_{mn}\} = \{0\} \quad (33)$$

We use condensation techniques to decouple the movements in the plane  $u_0(x, y)$  and  $v_0(x, y)$  to the transverse displacements  $w_0^b(x, y)$  and  $w_0^s(x, y)$  Then Eq. (33) reduces to

$$\begin{bmatrix} \underline{R}_{33} - F_x(\alpha^2 + \xi \beta^2) & \underline{R}_{34} - F_x(\alpha^2 + \xi \beta^2) \\ \underline{R}_{43} - F_x(\alpha^2 + \xi \beta^2) & \underline{R}_{44} - F_x(\alpha^2 + \xi \beta^2) \end{bmatrix} \begin{Bmatrix} W_{mn}^b \\ W_{mn}^s \end{Bmatrix} = \begin{Bmatrix} 0 \\ 0 \end{Bmatrix} \quad (34)$$

Then the critical thermal change  $\Delta T_{cr}$  that causes the plate to buckle is obtained according to the type of temperature distribution across the thickness, as shown in Table 3:

With  $\underline{R}_{ij}$  are the new terms after condensation such that:

$$\begin{aligned}
\underline{R}_{33} &= R_{33} - R_{13} \frac{R_{13}R_{22} - R_{12}R_{23}}{R_{11}R_{22} - R_{12}R_{12}} - R_{23} \frac{R_{11}R_{23} - R_{12}R_{13}}{R_{11}R_{22} - R_{12}R_{12}} \\
\underline{R}_{34} &= R_{34} - R_{14} \frac{R_{13}R_{22} - R_{12}R_{23}}{R_{11}R_{22} - R_{12}R_{12}} - R_{24} \frac{R_{11}R_{23} - R_{12}R_{13}}{R_{11}R_{22} - R_{12}R_{12}} \\
\underline{R}_{43} &= R_{34} - R_{13} \frac{R_{14}R_{22} - R_{12}R_{24}}{R_{11}R_{22} - R_{12}R_{12}} - R_{23} \frac{R_{11}R_{24} - R_{12}R_{14}}{R_{11}R_{22} - R_{12}R_{12}} \\
\underline{R}_{44} &= R_{44} - R_{14} \frac{R_{14}R_{22} - R_{12}R_{24}}{R_{11}R_{22} - R_{12}R_{12}} - R_{24} \frac{R_{11}R_{24} - R_{12}R_{14}}{R_{11}R_{22} - R_{12}R_{12}}
\end{aligned}$$

And the terms  $\kappa_{utr} = \frac{E_2 \alpha_0}{1-\nu_{12}} \int_{-h/2}^{h/2} dz$ ,  $\kappa_{ltr} = \frac{E_2 \alpha_0}{1-\nu_{12}} \int_{-h/2}^{h/2} \left(\frac{1}{2} + \frac{z}{h}\right) dz$  and  $\kappa_{str} = \frac{E_2 \alpha_0}{1-\nu_{12}} \int_{-h/2}^{h/2} \left[1 - \right.$

$$\cos\left(\frac{\pi}{4} + \frac{z\pi}{h}\right) dz.$$

#### 4.3 Free vibration analysis of laminated composite plates

According to the Navier technique adopted in this study, the system of equations Eq. (28) in the case of free vibration analysis is simplified by eliminating any transverse and thermal loading, in which case the problem will turn into an eigenvalue problem  $([\bar{R}] - \omega^2[M])\{d_{mn}\} = \{0\}$ . In order to have another solution than the trivial one  $\{d_{mn}\} = 0$ , it is necessary to cancel the determinant

$$\det([\bar{R}] - \omega^2[M]) = 0 \quad (35)$$

The solution of the eigenvalue problem Eq. (35) gives for each free vibration mode  $(m, n)$  a natural frequency of transverse vibration of the laminated composite plate under study. These natural frequencies are given in the following non-dimensional form

$$\bar{\omega} = \omega_{mn}(b^2/\pi^2)\sqrt{\rho h/D_{22}} \quad (36)$$

## 5. Numerical results and interpretations

To handle the proposed methodology, a plate made of laminated composite materials is considered. The Young's moduli, Poisson's ratios and thermal expansion coefficients are given in Table 1. The general approaches presented in the previous sections for the analysis of the thermal stability of the plate and their free vibration under uniform, linear and sinusoidal temperature variations through the thickness are illustrated in this section using numerical manipulations. The initial temperature will be set at  $T_i = 25$  C.

### 5.1 Validation of the theoretical approach adopted

In this section, we will compare the critical thermal loads  $\Delta T_{cr}$  and the fundamental natural frequency of vibration,  $\omega_{11}$ . The laminations studied are specially orthotropic, cross-ply antisymmetric and angle-ply antisymmetric. The only external load applied is a thermal load. The results obtained are compared with existing results in the literature to determine the accuracy of the proposed model. The verification is done for an increasing number of layers  $N_c = 2, 8$  and 12 layers.

All the results in Table 4 are compared with those found by Reddy's third order shear deformation plate theory HPT (Reddy 1984) and Touratier's sinusoidal shear deformation plate theory (SPT) (Touratier 1991). So, from this survey we observe that there is a similarity or almost similarity of the model proposed in this study and those existing in the literature. With a numerical comparison in terms of error, we can conclude from Table 4 that: The critical buckling temperatures found, using the proposed model, are scattered around of Reddy's model (HPT) with an average relative error of  $\Delta(\Delta T_{cr}) = 3.99\%$  and with an error of  $\Delta(\Delta T_{cr}) = 3.64\%$  for the results returned by the Touratier model (SPT). While, the fundamental pulses are found with an accuracy with respect to the (HPT) and (SPT) models successively of  $\Delta(\omega_{11}) = 1.03\%$  and  $\Delta(\omega_{11}) = 0.97\%$ .

Table 4 Validation of the methodology adopted in this study ( $E_1/E_2 = 40$ ,  $a/h = 10$  and  $a/b = 1$ )

Size	Theory	Especially orthotropic			Antisymmetric crosses			Antisymmetrical angular		
		$N_c = 2$	$N_c = 8$	$N_c = 12$	$N_c = 2$	$N_c = 8$	$N_c = 12$	$N_c = 2$	$N_c = 8$	$N_c = 12$
$\Delta T_{cr}$	Present	1.2583	1.1965	1.2584	0.8785	1.1582	1.1154	1.0254	1.5692	1.5895
	HPT	1.1868	1.1868	1.1868	0.8536	1.1051	1.1778	1.0671	1.5173	1.6421
	Error%	5,68	0,81	5,69	2,83	4,58	5,59	4,07	3,31	3,31
	SPT	1.2847	1.1847	1.1847	0.8524	1.1033	1.1757	1.0680	1.5151	1.6381
	Error%	2,10	0,99	5,86	2,97	4,74	5,41	4,15	3,45	3,06
$\omega_{11}$	Present	84.265	80.695	80.253	31.985	41.325	42.986	47.325	65.369	71.123
	HPT	84.511	80.511	81.048	32.903	41.527	43.752	47.636	66.144	70.575
	Error%	0,29	0,23	0,99	2,87	0,49	1,78	0,66	1,19	0,77
	SPT	84.003	80.945	80.945	32.824	41.463	43.693	47.683	66.238	70.694
	Error%	0,31	0,31	0,86	2,62	0,33	1,64	0,76	1,33	0,60

Table 5 The non-dimensional critical thermal loading  $\Delta T_{cr}$  of an antisymmetric plate with angular folds  $\theta$ 

$\frac{a}{h}$	$N_c = 2$ nappies			$N_c = 8$ nappies			$N_c = 12$ nappies		
	$\frac{E_1}{E_2} = 1$	$\frac{E_1}{E_2} = 20$	$\frac{E_1}{E_2} = 40$	$\frac{E_1}{E_2} = 1$	$\frac{E_1}{E_2} = 20$	$\frac{E_1}{E_2} = 40$	$\frac{E_1}{E_2} = 1$	$\frac{E_1}{E_2} = 20$	$\frac{E_1}{E_2} = 40$
2	15.3934	32.6073	39.1100	21.5943	36.4349	52.3728	23.0038	37.1694	54.4296
4	4.1859	9.5968	12.2988	5.9058	10.7326	16.4568	6.3785	11.0224	17.4483
20	0.1616	0.3974	0.5284	0.2330	0.4459	0.7114	0.2539	0.4597	0.7632

## 5.2 Parametric study

A parametric study is needed to see the effect of different types of coupling on the critical temperature value causing the thermo-elastic instability of the plate, as well as on the fundamental free vibration frequency. Similarly, for other parameters such as anisotropy, slenderness and aspect ratio of the plate and finally the lamination angle. This study also compares the responses of plates with specially orthotropic and antisymmetric lamination, and finally we will conclude this parametric study by extracting the effect of the temperature distribution through the plate thickness.

### 5.2.1 The critical buckling temperature of laminated composite plates

In this first manipulation (Table 5), the thermal behaviour (critical thermal load  $\Delta T_{cr}$ ) of an antisymmetric, square simply supported laminated composite plate is studied, we will consider three different plate schemes: ( $N_c = 2$  layers :  $-30/30$ ), ( $N_c = 8$  layers :  $(-30/30)_{4as}$ ) and ( $N_c = 12$  layers :  $(-30/30)_{6as}$ ) (the subscript 4as means that the plate consists of 4 pairs of layers  $(-30/30)$  symmetrically arranged), these patterns are studied in terms of the anisotropy ratio  $E_1/E_2$  and the slenderness ratio  $a/h$  as presented in Table 5.

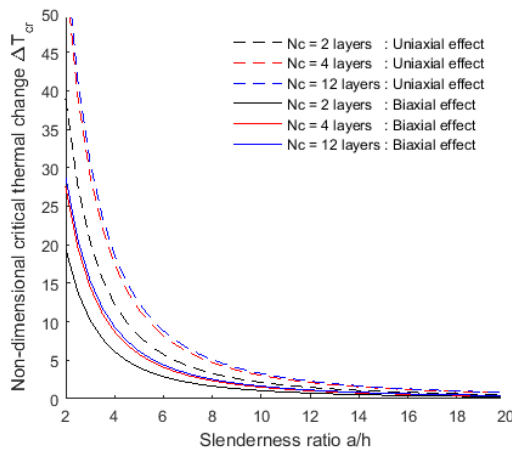
In Table 6, the thermal behaviour (critical thermal load  $\Delta T_{cr}$ ) of a simply supported antisymmetric cross-ply composite plate with square layers will be studied.  $N_c$  simply supported, will be studied. The study has been done for the three temperature distributions through the thickness of the plate (UTR: uniform distribution, LTR: linear distribution and STR: sinusoidal distribution). These case studies are manipulated for anisotropy  $E_1/E_2$  and slenderness ratio  $a/h = 20$ .

Table 6 The non-dimensional critical thermal loading  $\Delta T_{cr}$  of an antisymmetric two-ply plate

$\frac{E_1}{E_2}$	Uniform distribution		Linear distribution		Sinusoidal distribution	
	$a = b = 1$	$a = b = 4$	$a = b = 1$	$a = b = 4$	$a = b = 1$	$a = b = 4$
1	<b>38.6552</b>	<b>3.8665</b>	<b>77.2990</b>	<b>7.7216</b>	<b>70.2920</b>	<b>7.0217</b>
20	<b>45.6409</b>	<b>4.9789</b>	<b>91.2704</b>	<b>9.9464</b>	<b>82.9969</b>	<b>9.0448</b>
40	<b>56.1980</b>	<b>6.8620</b>	<b>112.3845</b>	<b>13.7127</b>	<b>102.1971</b>	<b>12.4696</b>

Table 6 The non-dimensional critical thermal loading  $\Delta T_{cr}$  of an antisymmetric cross-ply plate

Heat distribution	Number of layers $N_c$	Uni-axial thermal effect			Bi-axial thermal effect		
		$a/b = 1$	$a/b = 2$	$a/b = 4$	$a/b = 1$	$a/b = 2$	$a/b = 4$
Uniform UTR	2	<b>2.2237</b>	<b>1.0760</b>	<b>0.8624</b>	<b>1.1118</b>	<b>0.8608</b>	<b>0.8117</b>
	8	<b>2.7877</b>	<b>1.4153</b>	<b>1.1817</b>	<b>1.3939</b>	<b>1.1322</b>	<b>1.1122</b>
	12	<b>2.8099</b>	<b>1.4382</b>	<b>1.2040</b>	<b>1.4049</b>	<b>1.1506</b>	<b>1.1331</b>
Linear LTR	2	<b>4.4471</b>	<b>2.1518</b>	<b>1.7246</b>	<b>2.2235</b>	<b>1.7214</b>	<b>1.6231</b>
	8	<b>5.5752</b>	<b>2.8303</b>	<b>2.3631</b>	<b>2.7875</b>	<b>2.2642</b>	<b>2.2241</b>
	12	<b>5.6196</b>	<b>2.8763</b>	<b>2.4077</b>	<b>2.8097</b>	<b>2.3010</b>	<b>2.2661</b>
Sine wave STR	2	<b>4.0440</b>	<b>1.9567</b>	<b>1.5683</b>	<b>2.0219</b>	<b>1.5653</b>	<b>1.4760</b>
	8	<b>5.0699</b>	<b>2.5737</b>	<b>2.1489</b>	<b>2.5348</b>	<b>2.0589</b>	<b>2.0225</b>
	12	<b>5.1102</b>	<b>2.6155</b>	<b>2.1895</b>	<b>2.5550</b>	<b>2.0924</b>	<b>2.0606</b>



$T_i$  Initial temperature  
 $N_c$  Number of layers making up the plate

Hint for Figure 4:  
 UTR: Uniform temperature rise  
 LTR: Linear temperature increase  
 STR: Sinusoidal temperature increase

Hint for Figure 9:  
 SO: Specially orthotropic  
 SC : Antisymmetrical with cross folds  
 SA: Antisymmetric with angular folds

Fig. 3 Variation of the critical temperature  $\Delta T_{cr}$  as a function of the ratio  $a/h$  with  $N_c$  and the direction of thermal loading as parameters

The parametric study of the thermoelastic instability (determination of the critical thermal loading  $\Delta T_{cr}$ ) as a function of the aspect ratio of the plate  $a/b$  the number of layers  $N_c$  constituting an antisymmetric cross-ply plate and the direction of the thermal field effect. This study is done for all three types of temperature distribution through the thickness of the plate. The results in Table 6 show some of the results of this study. In this case we will set the anisotropy of the plate to  $E_1/E_2 = 40$  and a slenderness of  $a/h = 20$ .

The graphical illustrations of the non-dimensional critical thermal loading  $\Delta T_{cr}$  as a function of slenderness  $a/h$  or anisotropy  $E_1/E_2$  of a plate with different laminations are presented in Figs. 3,

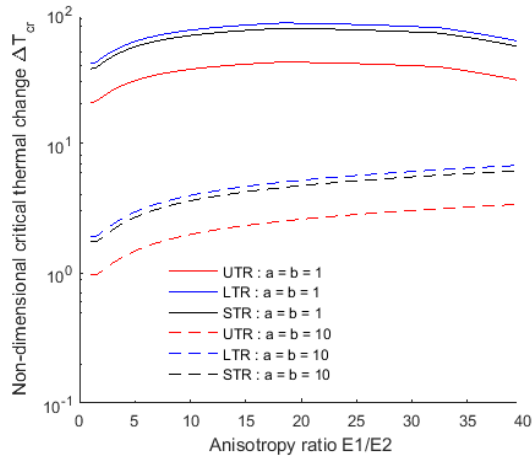


Fig. 4 Variation of the critical temperature  $\Delta T_{cr}$  as a function of the ratio  $E_1/E_2$  with plate size and temperature distribution as parameters

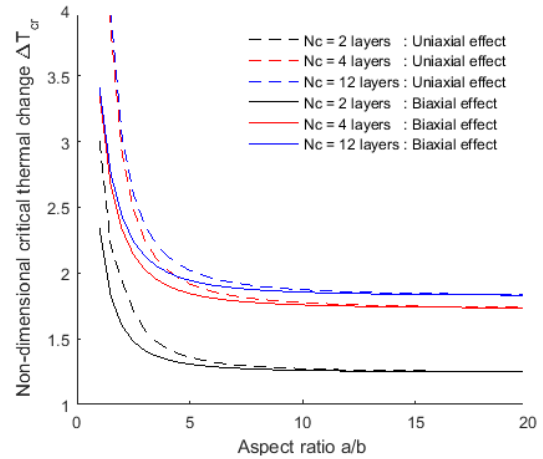


Fig. 5 Variation of the critical temperature  $\Delta T_{cr}$  as a function of the ratio  $a/b$  with  $N_c$  and the direction of thermal loading as parameters

4 and 5. The study parameters are the number of layers  $N_c$ , the temperature distribution through the thickness or the uni-axial or bi-axial temperature direction  $T(z)$ .

The influence of the considered thermal field on the thermoelastic instability of a laminated composite plate is shown in Fig. 3.  $\Delta T_{cr}$  decreases exponentially with increasing ratio  $a/h$ . These curves show that the critical temperature difference decreases exponentially with increasing ratio, so we can say that the thermal shear stresses have the effect of increasing the critical buckling temperature of the plate (i.e., in the case of  $N_c$  decreases). Also, we notice that the difference in the critical temperature  $\Delta T_{cr}$  increases if we replace the uni-axial effect of the thermal field by the bi-axial one.

From Fig. 4, we observe a significant difference between the critical buckling temperature difference of an antisymmetric cross-ply plate if the dimensions of the sides of the square plate are increased by a factor of 10. Similarly, this difference increases with increasing anisotropy ratio  $E_1/E_1$ .

In Fig. 5 we have drawn representative curves of the thermoelastic instability of a laminated composite plate as a function of the aspect ratio of the plate, thus the difference in the critical temperature  $\Delta T_{cr}$  decreases exponentially as the ratio increases  $a/b$ . If we take into account the number of layers  $N_c$  we notice that the critical buckling temperature increases with the increase of the number of layers, i.e., the different types of couplings are causes that accelerate the thermoelastic instability of a laminated composite material plate.

### 5.2.2 Free vibration analysis of laminated composite plates

The results obtained for the natural fundamental free vibration frequency of a laminated composite plate are given in Tables 7 and 8, the plate is assumed to be square and single supported under a linearly distributed thermal load. In Table 7, we have recorded the non-dimensional free vibration pulsation  $\omega_{11}$  of an antisymmetric plate with two angular plies, the study parameters are the number of layers  $N_c$  the anisotropy ratio  $E_1/E_2$  and the lamination angle  $\theta$ . Table 8 shows a comparison of the non-dimensional free vibration pulsation  $\omega_{11}$  for the three types of lamination

Table 7 The non-dimensional free vibration pulsation  $\omega_{11}$  of an antisymmetric square plate with two angular folds of angle  $\theta$  with  $a/h = 20$  and  $N_c = 8$  layers

Angle	$N_c = 2$ nappies			$N_c = 8$ nappies			$N_c = 12$ nappies		
	$\frac{E_1}{E_2} = 1$	$\frac{E_1}{E_2} = 20$	$\frac{E_1}{E_2} = 40$	$\frac{E_1}{E_2} = 1$	$\frac{E_1}{E_2} = 20$	$\frac{E_1}{E_2} = 40$	$\frac{E_1}{E_2} = 1$	$\frac{E_1}{E_2} = 20$	$\frac{E_1}{E_2} = 40$
$\theta = 45^\circ$	<b>1.1673</b>	<b>2.7969</b>	<b>2.9956</b>	<b>1.7253</b>	<b>3.4178</b>	<b>4.2351</b>	<b>1.8836</b>	<b>3.5940</b>	<b>4.5865</b>
$\theta = 30^\circ$	<b>1.6868</b>	<b>2.3544</b>	<b>2.3436</b>	<b>2.3238</b>	<b>2.7707</b>	<b>3.1462</b>	<b>2.5051</b>	<b>2.8899</b>	<b>3.3762</b>
$\theta = 75^\circ$	<b>3.3502</b>	<b>2.1467</b>	<b>2.1133</b>	<b>3.8966</b>	<b>2.2847</b>	<b>2.3889</b>	<b>4.0546</b>	<b>2.2847</b>	<b>2.3889</b>

Table 8 Comparison of non-dimensional free vibration pulsation  $\omega_{11}$  for the three types of plate laminations with eight layers

Heat distribution	$\frac{a}{b}$	Especially orthotropic plate		Anti-symmetrical cross-ply plate		Antisymmetrical plate with angular folds $\theta = 45^\circ$	
		$\frac{E_1}{E_2} = 25$	$\frac{E_1}{E_2} = 40$	$\frac{E_1}{E_2} = 25$	$\frac{E_1}{E_2} = 40$	$\frac{E_1}{E_2} = 25$	$\frac{E_1}{E_2} = 40$
Uniform	5	1.0445	1.1451	0.6007	0.5193	0.6526	0.5870
UTR	10	4.1925	4.6060	2.3965	8.6644	2.5904	2.3227
Linear	5	1.0444	1.1450	0.6006	0.5192	0.6525	0.5869
LTR	10	4.1920	4.6054	2.3961	8.6644	2.5900	2.3224
Sine wave	5	1.0444	1.1450	0.6006	0.5192	0.6525	0.5869
STR	10	4.1920	4.6055	2.3962	8.6644	2.5900	2.3224

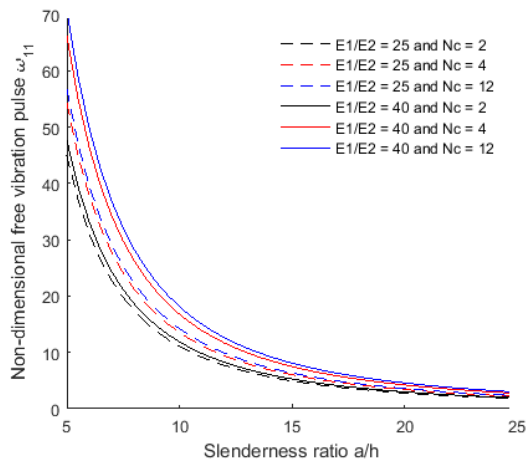


Fig. 6 Variation of the natural frequency  $\omega_{11}$  as a function of the ratio  $a/h$  with  $N_c$  and the anisotropy ratio  $E_1/E_2$  as parameters

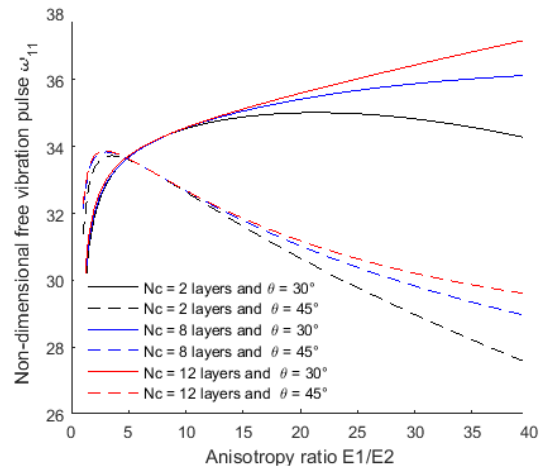


Fig. 7 Variation of the natural frequency  $\omega_{11}$  as a function of the ratio  $E_1/E_2$  with  $N_c$  and the stratification angle  $\theta$  as parameters

(especially orthotropic, antisymmetric cross-ply and antisymmetric angle-ply) of plates with eight layers.  $\theta = 45^\circ$ ) of plates with eight layers.

The graphical illustrations of the non-dimensional free vibration pulsation  $\omega_{11}$  as a function of the slenderness ratio  $a/h$ , anisotropy  $E_1/E_2$  or aspect ratio  $a/b$  of an antisymmetric plate with angular folds are presented successively in Figs. 6, 7 and 8. The study parameters are the number

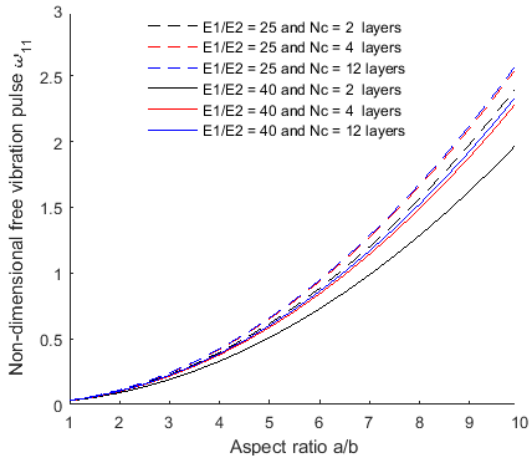


Fig. 8 Variation of the natural frequency  $\omega_{11}$  as a function of the ratio  $a/b$  with  $N_c$  and the anisotropy  $E_1/E_2$  as parameters

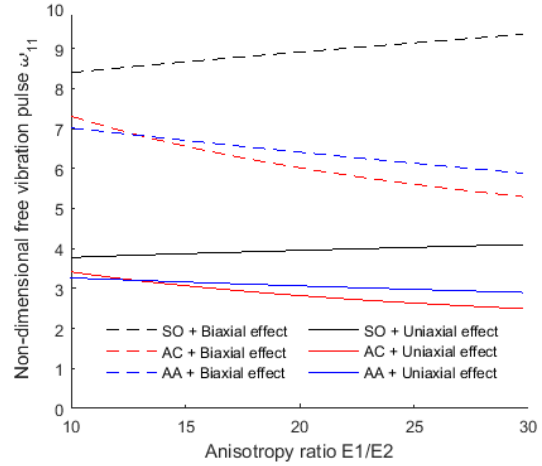


Fig. 9 Variation of  $\omega_{11}$  as a function of the ratio  $E_1/E_2$  with the direction of thermal loading and the type of stratification as parameters

of layers  $N_c$  the anisotropy ratio  $E_1/E_2$  or the lamination angle  $\theta$ .

Fig. 6 shows the effects of the slenderness ratio  $a/h$  on the free vibration pulsation of the plates for linear thermal loading. It can be seen that, irrespective of the number of layers and also for different anisotropy ratios, the pulsation for the (1,1) mode decreases exponentially with increasing ratio  $a/h$  for all types of thermal loading. It can also be seen from Fig. 7 that  $\omega_{11}$  increases with increasing ratio  $E_1/E_2$  in the case of stratification angle  $\theta = 30^\circ$  and decreases in the case of  $\theta = 45^\circ$ .

From the curves in Fig. 6 we also notice that plates with a larger anisotropy ratio vibrate with larger pulsations, so couplings in the plate have an effect of decreasing the free vibration frequency of the plate.  $\omega_{11}$ . Also the couplings in the plate have an effect of decreasing the free vibration frequency of the plate. While in Fig. 7, the free pulsations of the plate are smallest for  $\theta = 45^\circ$  and start to increase as  $\theta$  away from  $45^\circ$ .

Fig. 8 shows the variation of the fundamental free vibration pulsation of an antisymmetric cross-ply plate as a function of the  $a/b$  for two values of anisotropy  $E_1/E_2 = 25, 40$  and different layering schemes (different number of layers), this study shows that the pulsation becomes larger if the length of the plate becomes greater than its width, furthermore, coupling has an effect of decreasing this pulsation.

It can be seen from the curves in Fig. 9 that specially orthotropic laminated plates have the highest pulsations, while the antisymmetric cross-ply laminated plates vibrate with the lowest frequencies. For all types of laminations the free vibration pulsations are small in the uni-axial thermal loading case compared to the bi-axial cases.

## 6. Conclusions

The critical temperature difference triggering buckling and free vibration of simply supported laminated plates was analyzed by running a refined four-variable plate theory. This study analyzed

the effect of different types of thermal loading on a laminated composite plate in terms of thermo-elastic stability and free vibration pulsation, and showed, firstly, that the plate is susceptible to buckling under the action of this thermal field, whereas, its free vibration is not much affected in the same temperature range. From these activities we can conclude that: The critical buckling temperature difference obtained increases with the presence of different types of coupling, and also decreases with increasing slenderness ratio  $a/h$  and aspect ratio  $a/b$ . The free vibration pulsation is little influenced by the thermal field, so it decreases with increasing slenderness ratio  $a/h$  while it increases with aspect ratio  $a/b$ . In the case of especially orthotropic laminations, the free pulsation of the (1,1) mode is greater than in antisymmetrical laminations.

### Acknowledgement

I thank all the pedagogical and administrative staff of Sidi Mohamed Ben Abdellah University, 30040 Fez, Morocco for the pedagogical atmosphere they brought to the research.

### Reference

- Abdoun, F. and Azrar, L. (2020), "Thermal buckling and vibration of laminated composite plates with temperature dependent properties by an asymptotic numerical method", *Int. J. Comput. Meth. Eng. Sci. Mech.*, **21**(1), 43-57. <https://doi.org/10.1080/15502287.2020.1729899>.
- Adim, B., Daouadji, T.H., Abbas, B. and Rabahi, A. (2016), "Buckling and free vibration analysis of laminated composite plates using an efficient and simple higher order shear deformation theory", *Mech. Industry*, **17**(5), 512. <https://doi.org/10.1051/meca/2015112>.
- Álvarez, J.G., Abramovich, H. and Bisagni, C. (2022), "Vibration-buckling tests on heated composite plates", *J. Sound Vib.*, **536**, 117145. <https://doi.org/10.1016/j.jsv.2022.117145>.
- Barron, R.F. and Barron, B.R. (2011), *Design for Thermal Stresses*, John Wiley & Sons.
- Bouazza, M., Becheri, T., Boucheta, A. and Benseddiq, N. (2016), "Thermal buckling analysis of nanoplates based on nonlocal elasticity theory with four-unknown shear deformation theory resting on Winkler-Pasternak elastic foundation", *Int. J. Comput. Meth. Eng. Sci. Mech.*, **17**(5-6), 362-373. <https://doi.org/10.1080/15502287.2016.1231239>.
- Chen, L.W. and Chen, L.Y. (1989), "Thermal buckling behavior of laminated composite plates with temperature-dependent properties", *Compos. Struct.*, **13**(4), 275-287. [https://doi.org/10.1016/0263-8223\(89\)90012-3](https://doi.org/10.1016/0263-8223(89)90012-3).
- Ebrahimi, F., Nouraei, M., Dabbagh, A. and Rabczuk, T. (2019), "Thermal buckling analysis of embedded graphene-oxide powder-reinforced nanocomposite plates", *Adv. Nano Res.*, **7**(5), 293-310. <https://doi.org/10.12989/anr.2019.7.5.293>.
- Foroutan, K., Shaterzadeh, A. and Ahmadi, H. (2020), "Nonlinear static and dynamic hygrothermal buckling analysis of imperfect functionally graded porous cylindrical shells", *Appl. Math. Model.*, **77**, 539-553. <https://doi.org/10.1016/j.apm.2019.07.062>.
- Gutiérrez Álvarez, J. and Bisagni, C. (2021), "A study on thermal buckling and mode jumping of metallic and composite plates", *Aerosp.*, **8**(2), 56. <https://doi.org/10.3390/aerospace8020056>.
- Hammed, M.B. and Majeed, W.I. (2019), "Free vibration analysis of laminated composite plates with general boundary elastic supports under initial thermal load", *Al-Khwarizmi Eng. J.*, **15**(4), 23-32. <https://doi.org/10.22153/kej.2019.09.004>.
- Jeyaraj, P. (2013), "Buckling and free vibration behavior of an isotropic plate under nonuniform thermal load", *Int. J. Struct. Stab. Dyn.*, **13**(03), 1250071. <https://doi.org/10.1142/S021945541250071X>.
- Kobayashi, H. and Sonoda, K. (1991), "Vibration and buckling of tapered rectangular plates with two

- opposite edges simply supported and the other two edges elastically restrained against rotation”, *J. Sound Vib.*, **146**(2), 323-337. [https://doi.org/10.1016/0022-460X\(91\)90766-D](https://doi.org/10.1016/0022-460X(91)90766-D).
- Leissa, A.W. (1987), “A review of laminated composite plate buckling”, *Appl. Mech. Rev.*, **40**(5), 575-591. <https://doi.org/10.1115/1.3149534>.
- Madenci, E., Özkılıç, Y.O. and Gemi, L. (2020), “Buckling and free vibration analyses of pultruded GFRP laminated composites: Experimental, numerical and analytical investigations”, *Compos. Struct.*, **254**, 112806. <https://doi.org/10.1016/j.compstruct.2020.112806>.
- Majeed, W.I. and Sadiq, I.A. (2022), “Thermal buckling of laminated plates using modified Mantari function”, *J. Mech. Eng. (JMecE)*, **19**(3), 205-220. <https://doi.org/10.24191/jmeche.v19i3.19813>.
- Ounis, H., Tati, A. and Benchabane, A. (2014), “Thermal buckling behavior of laminated composite plates: A finite-element study”, *Front. Mech. Eng.*, **9**, 41-49. <https://doi.org/10.1007/s11465-014-0284-z>
- Owhadi, A. and Samsam Shariat, B. (2009), “Stability analysis of symmetric laminated composite plates with geometric imperfections under longitudinal temperature gradient”, *J. Mech.*, **25**(2), 161-165. <https://doi.org/10.1017/S1727719100002616>.
- Panda, S.K. and Katariya, P.V. (2015), “Stability and free vibration behaviour of laminated composite panels under thermo-mechanical loading”, *Int. J. Appl. Comput. Math.*, **1**, 475-490. <https://doi.org/10.1007/s40819-015-0035-9>.
- Patro, S.S., Sutradhar, D., Behera, R.K. and Sharma, N. (2018), “Free vibration analysis of stiffened laminated composite plate in a thermal environment”, *IOP Conf. Ser.: Mater. Sci. Eng.*, **390**(1), 012040. <https://doi.org/10.1088/1757-899X/390/1/012040>.
- Prasad, N.E. and Wanhill, R.J. (2017), *Aerospace Materials and Material Technologies*, Springer, Singapore.
- Rasid, Z.A. and Yahaya, H. (2015), “The thermal instability analysis of functionally graded carbon nanotube composite plates using finite element method”, *Appl. Mech. Mater.*, **695**, 285-288. <https://doi.org/10.4028/www.scientific.net/amm.695.285>.
- Reddy, J.N. (1984), “A simple higher-order theory for laminated composite plates”, *J. Appl. Mech.*, **51**(4), 745-752. <https://doi.org/10.1115/1.3167719>.
- Rostamijavanani, A., Ebrahimi, M.R. and Jahedi, S. (2021), “Thermal post-buckling analysis of laminated composite plates embedded with shape memory alloy fibers using semi-analytical finite strip method”, *J. Fail. Anal. Prevent.*, **21**, 290-301. <https://doi.org/10.1007/s11668-020-01068-5>.
- Sayyad, A.S. and Ghugal, Y.M. (2014), “On the buckling of isotropic, transversely isotropic and laminated composite rectangular plates”, *Int. J. Struct. Stab. Dyn.*, **14**(07), 1450020. <https://doi.org/10.1142/S0219455414500205>.
- Sayyad, A.S., Shinde, B.M. and Ghugal, Y.M. (2016), “Bending, vibration and buckling of laminated composite plates using a simple four variable plate theory”, *Lat. Am. J. Solid. Struct.*, **13**, 516-535. <https://doi.org/10.1590/1679-78252241>.
- Shiau, L.C. and Wu, T.Y. (1997), “Free vibration of buckled laminated plates by finite element method”, *J. Vib. Acoust.*, **119**(4), 635. <https://doi.org/10.1115/1.2889774>.
- Shinde, B.M., Kawade, A.B. and Sayyad, A.S. (2013), “Thermal response of isotropic plates using hyperbolic shear deformation theory”, *Int. J. Adv. Technol. Civil Eng.*, **2**(1), 140-145.
- Shinde, B.M., Sayyad, A.S. and Kawade, A.B. (2013), “Thermal analysis of isotropic plates using hyperbolic shear deformation theory”, *Appl. Comput. Mech.*, **7**(2), 193-204. <http://doi.org/10.47893/IJATCE.2013.1068>.
- Sobhy, M. (2016), “An accurate shear deformation theory for vibration and buckling of FGM sandwich plates in hygrothermal environment”, *Int. J. Mech. Sci.*, **110**, 62-77. <https://doi.org/10.1016/j.ijmecsci.2016.03.003>.
- Sun, Y. (2021), “Buckling and vibration performance of a composite laminated plate with elastic boundaries subjected to local thermal loading”, *Shock Vib.*, **2021**, Article ID 5537946. <https://doi.org/10.1155/2021/5537946>.
- Touratier, M. (1991), “An efficient standard plate theory”, *Int. J. Eng. Sci.*, **29**(8), 901-916. [https://doi.org/10.1016/0020-7225\(91\)90165-Y](https://doi.org/10.1016/0020-7225(91)90165-Y).

- Trabelsi, S., Zghal, S. and Dammak, F. (2020), "Thermo-elastic buckling and post-buckling analysis of functionally graded thin plate and shell structures", *J. Brazil. Soc. Mech. Sci. Eng.*, **42**, 1-22. <https://doi.org/10.1007/s40430-020-02314-5>.
- Van Tung, H. (2015), "Thermal and thermomechanical postbuckling of FGM sandwich plates resting on elastic foundations with tangential edge constraints and temperature dependent properties", *Compos. Struct.*, **131**, 1028-1039. <https://doi.org/10.1016/j.compstruct.2015.06.043>.
- Yang, X., Fei, Q., Wu, S. and Li, Y. (2020), "Thermal buckling and dynamic characteristics of composite plates under pressure load", *J. Mech. Sci. Technol.*, **34**, 3117-3125. <https://doi.org/10.1007/s12206-020-0702-6>.
- Yang, Z., Liu, A., Yang, J., Fu, J. and Yang, B. (2020), "Dynamic buckling of functionally graded graphene nanoplatelets reinforced composite shallow arches under a step central point load", *J. Sound Vib.*, **465**, 115019. <https://doi.org/10.1016/j.jsv.2019.115019>.
- Yüksel, Y.Z. and Akbaş, Ş.D. (2018), "Free vibration analysis of a cross-ply laminated plate in thermal environment", *Int. J. Eng. Appl. Sci.*, **10**(3), 176-189. <https://doi.org/10.24107/ijeas.456755>.
- Zenkour, A.M. and Sobhy, M. (2010), "Thermal buckling of various types of FGM sandwich plates", *Compos. Struct.*, **93**(1), 93-102. <https://doi.org/10.1016/j.compstruct.2010.06.012>.
- Zhao, X., Zhu, W.D. and Li, Y.H. (2020), "Analytical solutions of nonlocal coupled thermoelastic forced vibrations of micro-/nano-beams by means of Green's functions", *J. Sound Vib.*, **481**, 115407. <https://doi.org/10.1016/j.jsv.2020.115407>.